Environment International 132 (2019) 105087

Contents lists available at ScienceDirect

Environment International

journal homepage: www.elsevier.com/locate/envint

Enzymatic degradation of extracellular DNA exposed to chlorpyrifos and chlorpyrifos-methyl in an aqueous system

Bing Yang[a,1], Chao Qin[a,1], Xiaojie Hu[a], Kang Xia[b], Chao Lu[a], Fredrick Owino Gudda[a], Zhao Ma[a], Yanzheng Gao[a,*]

[a] Institute of Organic Contaminant Control and Soil Remediation, College of Resources and Environmental Sciences, Nanjing Agricultural University, Nanjing 210095, P.R. China
[b] School of Plant and Soil Environmental Sciences, Virginia Polytechnic Institute and State University, Blacksburg, VA 24061, United States

ARTICLE INFO

Handling Editor: Hefa Cheng

Keywords:
Extracellular DNA
Deoxyribonuclease I (DNase I)
Organophosphorus
Pesticides
Spectroscopy
Molecular dynamics

ABSTRACT

The persistence of extracellular DNA (eDNA) is crucial for ensuring species diversity and ecological function in aquatic systems. However, scarce information exists about the impact of pesticides on eDNA, although they often co-exist in the aquatic environment. Using a variety of spectroscopic analyses, eDNA degradation and the associated alterations in DNA secondary structure was investigated by exposing DNase I to tested DNA in the presence of chlorpyrifos, a commonly used organophosphate pesticide. Molecular dynamics simulation was used to explore the weak interactions between the tested DNA and chlorpyrifos. The results indicated that chlorpyrifos significantly enhanced DNA degradation without affecting the enzyme activity of DNase I in an aqueous system. Spectroscopic experiments confirmed that chlorpyrifos and the analog chlorpyrifos-methyl could bind with DNA to cause the bases noncovalent stacking interaction. Molecular simulations further demonstrated that pesticide binding with DNA molecules caused widening of the DNA grooves and destruction of the hydrated layer, which enhanced DNA degradation. The findings presented herein provide novel insight into the genotoxicity and ecotoxicity of chlorpyrifos and chlorpyrifos-methyl, as well as their impacts on DNA persistence in aquatic environments.

1. Introduction

Extracellular DNA (eDNA) is released via cell lysis or egested by organisms as metabolic waste into the aquatic systems (Barnes et al., 2014; Ibáñez de Aldecoa et al., 2017). Approximately 0.03–88 μg of eDNA can be recovered per liter of natural water, with the sizes of the fragments ranging from 0.12 kb (7.75×10^4 Da) to 35.2 kb (2.32×10^7 Da), and their bioavailability can persist for 6.5–25 h in various aquatic environments (Matsui et al., 2001; Nielsen et al., 2007; Torti et al., 2015). The gene pools built from the continuous release of eDNA may be used for genetic recombination and genetic transformation in horizontal gene transfer (HGT), and contribute to evolution and speciation of prokaryotic organisms (Corinaldesi et al., 2005). The proportion of bacteria found to take up naked eDNA is approximately 1% of the validly described bacterial species (Thomas and Nielsen, 2005). Besides, eDNA is ubiquitous and pivotal in biofilm structural integrity, and the proximity and high cell density that are inherent to biofilms, providing a stable physical environment for cell-to-cell contacts that are important for HGT (Flemming et al., 2016; Whitchurch et al., 2002). Interestingly, eDNA in the biofilms can also be a source of DNA in HGT (Flemming et al., 2016). Hence, the persistence of eDNA plays a crucial role in maintaining species diversity and biological function within aquatic systems.

Many biotic and abiotic factors influence eDNA persistence and dynamics, therefore, the limits HGT frequency (Ponnuswamy et al., 2017; Thomas and Nielsen, 2005). The integrity of DNA released from the cells depends on the activity and location of nucleases and reactive chemicals. Deoxyribonuclease I (DNase I) is released along with eDNA into aquatic systems and can cleave eDNA into smaller duplex DNA fragments of about 400 bp (Bylemans et al., 2018; Demanèche et al., 2001). Okabe (Okabe and Shimazu, 2007) and Dick et al. (2010) have suggested that increased temperature, directly and indirectly, enhances eDNA degradation by denaturing DNA molecules and increasing enzyme activity. Borin et al. (2008) reported that hypersaline environments may affect the conformational stability of eDNA and restrict exonuclease activity, which may limit its degradation. Additionally,

* Corresponding author.
E-mail addresses: gaoyanzheng@njau.edu.cn, soilchem@njau.edu.cn (Y. Gao).
[1] Contributed equally to this work.

https://doi.org/10.1016/j.envint.2019.105087
Received 14 May 2019; Received in revised form 30 July 2019; Accepted 7 August 2019
Available online 17 August 2019

previous research have also shown that eDNA can avoid enzymatic stress through adsorption onto insoluble particles (e.g., clay minerals, sand, and humic substances) and thereby persist in the environment for a long period (Mao et al., 2014; Saeki et al., 2011). From the release of eDNA to degradation, the disturbance of exogenous substances is unknown. In order to adequately illuminate eDNA fate, it is necessary to investigate eDNA degradation with exogenous substances into account in the natural process as an integral.

The exogenous pollutants from anthropogenic activities have been increasingly released into the aquatic environment, coexisting with eDNA. Recent studies have shown that organic pollutants can affect the degradation of DNA by altering enzyme activity or DNA conformation. Pollutants such as phenol, bromobenzene, and chlorobenzene have been shown to significantly increase the enzyme activity of DNase I, resulting in enhanced DNA degradation in the marine environment (Popov et al., 2003); however, the mechanism of this reaction has not been revealed. Our previous study indicated that phenanthrene, pyrene, and hexachlorocyclohexanes caused DNA structural changes that decelerated or accelerated DNA degradation by DNase I (Kang et al., 2010; Qin et al., 2019). To this end, there is an urgent need to identify the contribution, if there are any, of relevant environment contaminants for further studies of eDNA persistence, and an in-depth study to understand the effects of DNA and DNase I from recognition to shear, in the presence of environmental contaminants.

Pesticides deserve a special attention because of their extensive use, their environmental persistence, and influence. Chlorpyrifos (CPY) is an organophosphorus pesticide that is extensively applied to a variety of food and feed crops (Trunnelle et al., 2014). In 2008, the market demand for CPY in China was 18,000 tons. A nationwide survey in the United States showed that CPY was detected in 9% of samples from > 10,000 streams, with documented concentrations reaching 0.33 μg/L (Williams et al., 2014). The half-life of CPY in pure water ranges from 29 to 74 days under standardized laboratory conditions (Kovačić and Medić, 2016). The analogous compound chlorpyrifos-methyl (CPYM) is also widely used on crops and cattle as a restricted agricultural pesticide in many countries (Hua et al., 2010). Both CPY and CPYM persist in farmlands and can be transported into the surface water system through runoff, presenting risks due to their toxicity in aquatic ecosystems (Giesy and Solomon, 2014; Koureas et al., 2012). A dearth of information has been uncovered on the effects of pesticides on DNA enzymatic degradation in aquatic systems. 3, 5, 6-trichloro-2-pyridinol, a secondary metabolite of CPY hasbeen shown to bind to DNA by groove binding and cause changes in DNA structure (Kashanian et al., 2012). However, the persistence of eDNA in aquatic systems, in the presence of these pesticides, has not been sufficiently investigated. Toward this end, the key challenge is to scale the interference of DNA deformation caused by pesticides on DNA degradation process.

Therefore, this study aimed to elucidate the effects and mechanism of DNA degradation through the binding of two organophosphorus pesticides to double-stranded DNA. The enzymatic degradation phenomena and processes of DNA exposed to DNase I and pesticides were determined by gel electrophoresis and ultraviolet-visible methods (UV–vis). Structural changes in DNA, due to binding with CPY and CPYM were confirmed using fluorescence and UV–vis, circular dichroism (CD), and Fourier-transform infrared (FTIR) spectroscopy techniques. Computational chemistry methods provided more details about molecular information on the degradation mechanism by calculating the interactions of DNA with CPY and CPYM.

2. Material and methods

2.1. Sample preparation

CPY and CPYM were purchased from Dr. Ehrenstorfer GmbH Co. (Augsburg, Germany). The general properties of CPY and CPYM are presented in Table S1 in the Supplementary information (SI). Salmon sperm DNA, a double-stranded DNA with an average molar mass of 1.3×10^6 Da (Tanaka and Okahata, 1996), was purchased from Sigma Chemical Co. (St. Louis, MO, USA). DNase I was purchased from Takara Bio Co. (Dalian, China). All other chemicals employed in this study were of analytical grade and without further purification. Deionized double-distilled water was used throughout the experiments. Stock solutions of CPY and CPYM were dissolved in methyl alcohol to obtain a final concentration of 1 g/L. The DNA stock solution (1 g/L) was prepared by dissolving DNA (100 mg) in 10 mmol/L Tris–HCl buffer (100 mL, pH 7.0) and stored at 4 °C. The DNase I working solution was diluted in buffer solution (10 mmol/L Tris–HCl (pH 7.0), 10 mmol/L $CaCl_2$, and 10 mmol/L $MgCl_2$) to 1 U/μL.

2.2. Experimental design

Enzymatic degradation phenomena of DNA by DNase I in the presence of pesticides was assayed using agarose gel electrophoresis. First, 10 μL of 1 g/L DNA solution was pipetted into a 200-μL tube, and a predetermined volume of CPY or CPYM solution was added to each tube to final concentrations of 0–2.0 or 0–4.0 mg/L, respectively. Tris–HCl (10 mmol/L, pH 7.0) was added to each tube to obtain a final volume of 99 μL, followed by incubation for 2 h at 4 °C. The incubated samples were then transferred to room temperature conditions, and 1 μL of the DNase I working solution described above was added to each tube, which was thoroughly mixed and incubated for 20 min at 37 °C. The reaction was stopped by adding 10 μL loading buffer (30 mmol/L EDTA, 50% (v/v) glycerol, 0.25% (w/v) xylene cyanol FF, and 0.25% (w/v) bromophenol blue), and followed by incubation in water bath at 85 °C for 2 min, then loaded the mixed sample into a well of the 3% w/v agarose gel plate, electrophoresis was run at 6 V/cm. The gel was then stained with ethidium bromide (EtBr) for 15 min, then collecting photos using a Bio-Rad imaging system and Quantity One software (Bio-Rad, Hercules, CA, USA). For this experiment, 11 concentrations of CPY or CPYM were used to determine the effects of CPY and CPYM on DNA enzymatic hydrolysis. Then, 9 concentrations of methanol as control were added to the DNA solution to rule out any effects of methanol on DNA degradation.

A real-time spectral experiment on DNA degradation was performed using a FLUOstar Optima plate reader (SpectraMax i3x; Molecular Devices, San Jose, CA, USA). Sample preparation was consistent with the experiment outlined above, and the concentration of DNase I was 0.5 U/100 μL. For the measurement, 200 μL of DNA and pesticide solution containing 1 U DNase I were added to each well of a quartz plate. The absorbance of each sample in the plate was measured at 260 nm for 30 min at 37 °C in 10-s intervals.

The enzymatic activity of DNase I was examined according to previously reported methods with some modifications (Tomar et al., 2014). The DNase I and pesticides were mixed with samples for 30 min at 37 °C to degrade the DNA. The activity of DNase I was positively correlated with the absorbance of the tested DNA solution. The detailed experimental procedures are described in SI.

2.3. Spectroscopic analysis

The UV–vis spectrum can be used for preliminary evaluation of the binding strength and mode of DNA with pesticides, while fluorescence quenching titration experiments can provide quantitative information about the binding strength of DNA–pesticide interactions. UV–vis spectrophotometric (Cary 5000; Varian, Palo Alto, CA, USA) experiments were conducted in Tris–HCl buffer (pH 7.0) at room temperature. The concentration of DNA was 10 mg/L, while the CPY and CPYM concentrations were 0–2.0 and 0–4.0 mg/L, respectively. After the addition of pesticides, all samples were allowed to stand for 2 h to reach equilibrium. Then, samples were transferred to 1-cm quartz cuvettes, and the UV absorption spectrum (220–300 nm) was measured in 1-nm intervals.

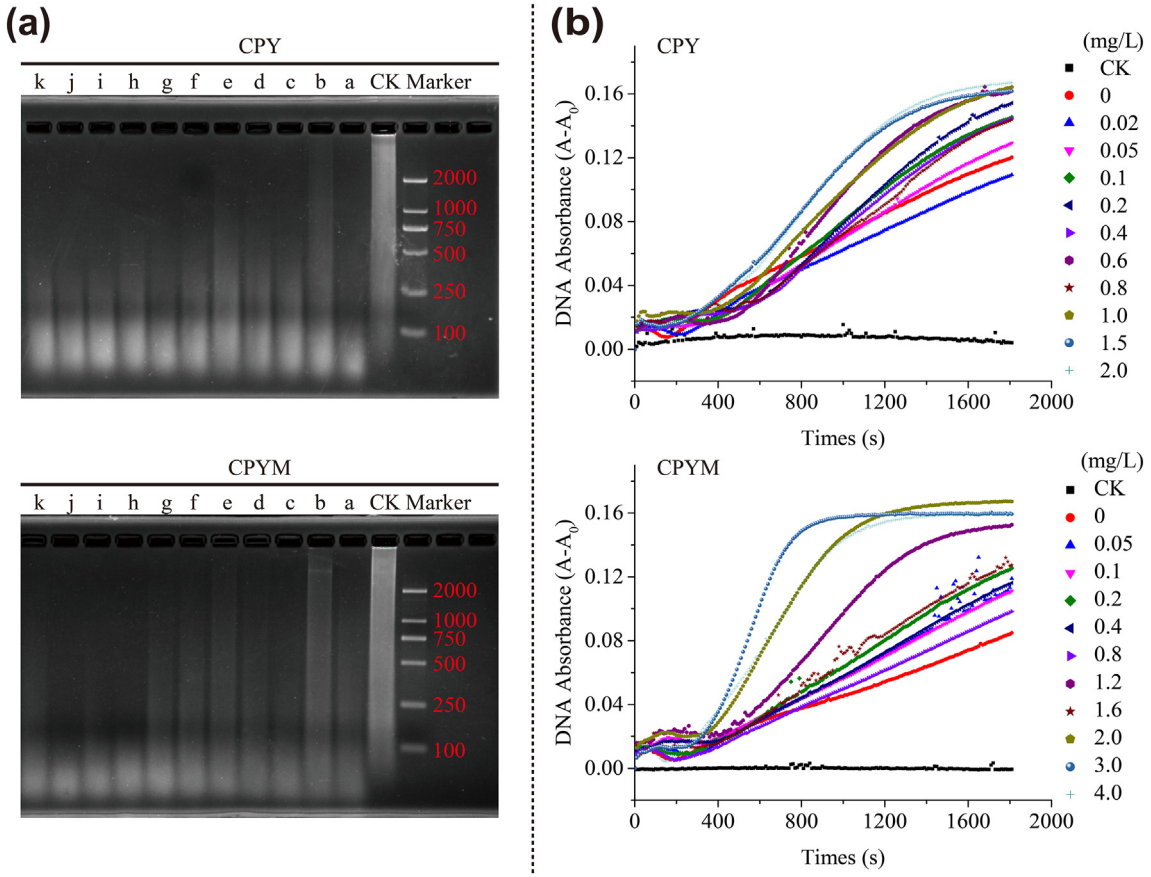

Fig. 1. Effects of the pesticides chlorpyrifos (CPY) or chlorpyrifos-methyl (CPYM) on DNA degradation. a, Gel electrophoresis of DNA fragments. CK represents the control treatment without DNase I. Letters a to k represent CPY concentrations of 0, 0.02, 0.05, 0.1, 0.2, 0.4, 0.6, 0.8, 1.0, 1.5, and 2.0 mg/L and CPYM concentrations of 0, 0.05, 0.1, 0.2, 0.4, 0.8, 1.2, 1.6, 2.0, 3.0, and 4.0 mg/L, respectively. b, Increase in DNA ultraviolet light absorbance caused by DNase I in the presence of CPY (top) and CPYM (bottom), with their concentrations presented on the right y–axis. A and A_0 represent DNA ultraviolet light absorbance in the absence and presence of DNase I, respectively.

The binding strengths of the pesticides to DNA were determined with fluorescence quenching titration experiments (Kang et al., 2015). The detailed experimental protocol is summarized in SI.

The binding mode or conformational changes of DNA with CPY and CPYM molecules can be derived using CD spectroscopy (Chirascan; Applied Photophysics, Leatherhead, UK). CD spectra were collected over a wavelength range of 210–350 nm at 25 °C in the absence and presence of pesticides. The concentration of DNA was 10 mg/L, and the final concentrations of CPY and CPYM were 0–2.0 and 0–4.0 mg/L, respectively. The spectrum of the buffer solution (10 mmol/L Tris–HCl, pH 7.0) was subtracted from the DNA and pesticide–DNA complex spectra for baseline correction. Solutions of pesticide–DNA complex were scanned in 0.5-cm (1-mL) quartz cuvettes.

FTIR was used to evaluate and characterize the chemical structures of DNA samples to determine the binding sites of a given DNA–pesticide combination. The respective final concentrations of CPY and CPYM were 2.0 and 4.0 mg/L, and the DNA concentration was 10 mg/L. After a 2-h static suspension treatment, the mixtures were dried at −65 °C. The dried samples were mixed with KBr at a ratio of 1:100. Then, the samples were tested using a FTIR spectrometer (NEXUS870; Nicolet, Madison, WI, USA). Plots of relative intensity (R_i) showed several peaks representing DNA in-plane vibrations of the adenine, thymine, guanine, and cytosine bases, as well as D-2-deoxyribose and phosphoric acid stretching vibrations, which were calculated using the following equation:

$$R_i = \frac{I_i}{I_{965}} \quad (1)$$

where I_i is the intensity of the absorption peak for pure or complexed DNA, and I_{965} is the intensity of the 965 cm^{-1} peak (internal reference).

2.4. Model computation

Molecular dynamics were conducted to confirm whether pesticides will affect DNA degradation via conformational changes. The three-dimensional structure of B-DNA dodecamer $d(CGCGAATTCGCG)_2$ was downloaded from the Protein Data Bank (PDB ID: 2B0K). The optimized geometries of CPY and CPYM were calculated with Gaussian 09 using the B3LYP/6-311G (d, p) basis sets. AutoDock software was used to dock the pesticide molecule to DNA and manually insert pesticide molecules into DNA base pairs (AT, GC) as the initial structure for molecular dynamics simulation (Morris et al., 2009). All water molecules were deleted, as they hinder proper docking. Non-polar hydrogen atoms were merged, and Kollman charges were added using MGLTools 1.5.6 (Morris et al., 1998). Molecular dynamics simulations were conducted using the GROMACS 2016.4 package (Páll et al., 2015) with the AMBER99SB force field for DNA and a customized force field for CPY and CPYM produced by Antechamber (Wang et al., 2006). The system was placed in a cube-shaped box under periodic boundary conditions containing specific TIP3P model water molecules neutralized with sodium ion counterions. System potential energy minimization was performed at 100 ps to relax the structure and avoid steric hindrance in further simulations. The pressure and temperature of the system were controlled at 1 atm and 298 K using NPT simulations (100 ps). The productive molecular dynamics trajectory was obtained for a time-period of 10 ns. Dynamic analysis and display of results were performed

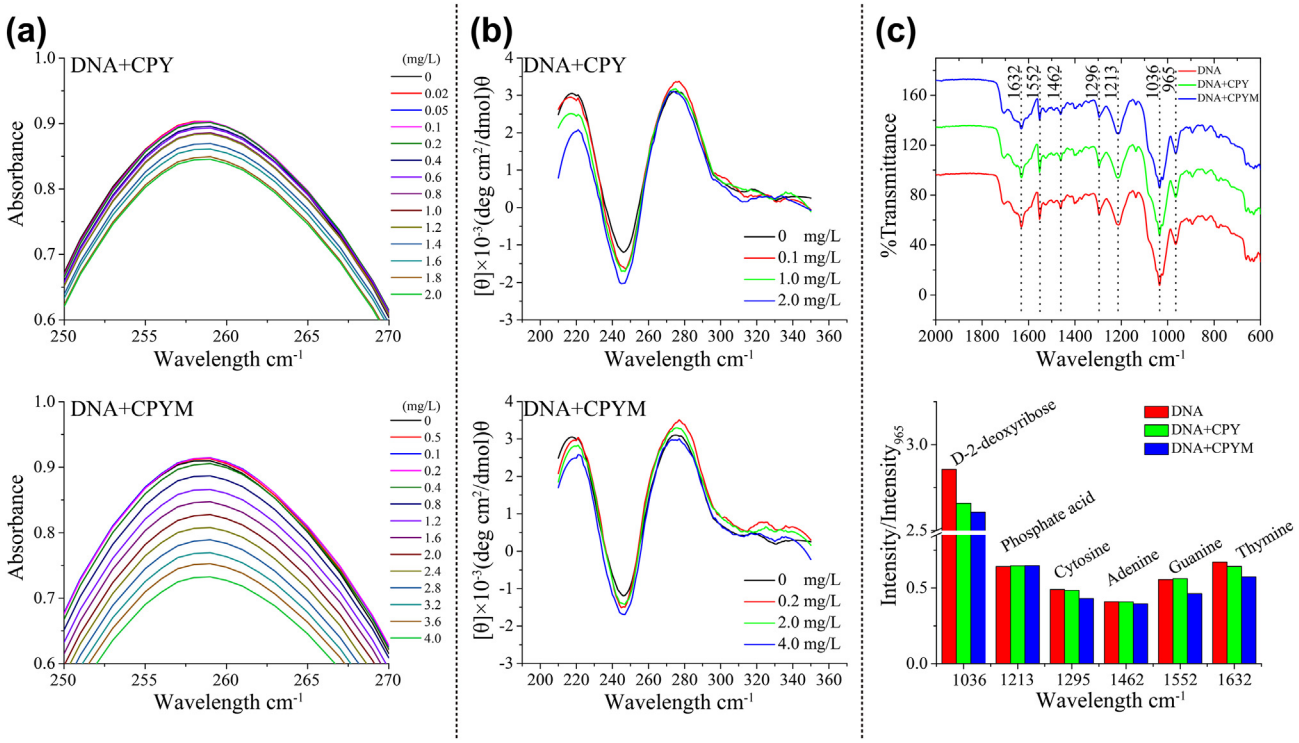

Fig. 2. Ultraviolet, circular dichroism, and Fourier-transform infrared (FTIR) spectral analyses confirming DNA structural changes in the presence of chlorpyrifos and chlorpyrifos-methyl. a, Ultraviolet spectra represent the direction of absorbance change with increasing pesticides concentrations. b, Circular dichroism spectra of DNA base stacking (275 nm) and right–handed helicity (246 nm) with increasing pesticide concentrations. c, FTIR spectra of DNA in the absence and presence of chlorpyrifos (CPY) and chlorpyrifos-methyl (CPYM). The bar graph of (c) shows the intensity ratio variations (R_i) for DNA in–plane vibrations at 1632 (thymine), 1552 (guanine), 1462 (adenine), 1295 (cytosine), 1213 (phosphate acid), and 1036 cm^{-1} (D–2–deoxyribose) in the absence and presence of CPY and CPYM.

using the GROMACS analysis module, VMD 1.9.3 software, Multiwfn Analyzer, Do_X3dna tool, and Origin 2016 software (Humphrey et al., 1996; Kumar and Grubmüller, 2015; Lu and Chen, 2012).

3. Results

3.1. Enzymatic degradation of DNA exposed to pesticides

To assess the effects of pesticides on enzymatic degradation of DNA at different CPY and CPYM concentrations, the DNA fragment size distribution and UV light absorbance over time exposed to CPY and CPYM were determined (Fig. 1).

In gel electrophoresis, DNA fragments travel due to the electric field from the sample-loading hole to the positive pole, and the fragment size is inversely proportional to the migration rate (Sambrook et al., 1989). Compared to the size distribution of pristine DNA fragments in the negative control (CK) without DNase I and pesticides, the presence of DNase I resulted in degradation of DNA into smaller fragments, most of which were < 2000 bp (Fig. 1a). In the presence of DNase I alongside CPY (0–2.0 mg/L) or CPYM (0–4.0 mg/L), smaller (< 500 bp) DNA fragments were observed (Fig. 1a). DNA fragments were decreased (smaller than 500 bp) with the increasing concentrations of CPY and CPYM. In Fig. S1, with increasing methanol concentrations, the lengths of degraded DNA fragments in the 9 samples ranged from 100 to 1000 bp, with no significant difference, which ruled out the effect of methanol on DNA degradation. This result indicates that CPY and CPYM enhanced DNA degradation by DNase I.

A previous study reported that when DNA degraded into small fragments, the concealed conjugated structure of folded long-chain DNA is exposed, resulting in greater UV absorbance at 260 nm by the exposed conjugated structure compared to undegraded DNA (Sun et al., 2017). An increasing UV absorbance at 260 nm was detected using a microplate reader during pesticide-mediated DNA degradation (Fig. 1b). During 30 min of degradation in the presence of DNase I, the UV absorbance of DNA increased from 0.120 to 0.167 as the CPY concentration increased from 0 to 2.0 mg/L. Increasing the CPYM concentration from 0 to 4.0 mg/L resulted in an increase in UV absorbance from 0.085 to 0.160. Thus, the increased UV absorbance at higher pesticide concentrations suggested that the tested pesticides significantly enhanced DNA degradation and that CPYM was more effective than CPY.

3.2. Effects of pesticides on DNase I activity

To identify the mechanism of pesticides-expedited enzymatic degradation of DNA, the effect of CPY and CPYM on the DNase I activity by the spectrophotometric experiments was carried out. As shown in Fig. S2, with increasing concentrations of pesticides, the absorbance of DNA enzymatic fragment did not increase or decrease obviously at 260 nm. Indicating the presence of pesticides did not significantly enhance DNase I activity compared to the treatment in which they were absent. Therefore, the observed enhancement of DNA degradation, in the presence of the two pesticides, could not be attributed to enhanced DNase I activity. Therefore, enhanced enzymatic degradation of DNA, in the presence of CPY or CPYM, is most likely caused by the deformation of DNA via interactions with the two pesticides, based on the physicochemical characteristics of DNA and both pesticides. Further investigations of binding and deformation between DNA and the pesticides are needed to guide the interpretation of promoted DNA degradation results.

3.3. Experimental binding of CPY and CPYM with DNA

Conjugated structures formed by the purine and pyrimidine bases of the tested DNA have a maximum UV absorption peak at ~260 nm. The fluctuation of absorbance at ~260 nm is due to the binding of small

molecules to DNA; the loose DNA double helix indicates a phenomenon referred to as hyperchromism, whereas the hypochromism likely resulted in the DNA helical structure contraction and deformation of DNA (Ma et al., 2015). The UV absorption spectra shown in Fig. 2a revealed hypochromism of DNA at a wavelength of 258 nm that increased with increasing concentrations of each pesticide. In comparison to the control treatment containing DNA without pesticides, the maximum UV absorbance intensity at 258 nm decreased by 6.32% and 19.58% in treatments combining with DNA and 2.0 mg/L CPY and 4.0 mg/L CPYM, respectively, indicating a hypochromicity of the tested double-stranded DNA in the presence of both pesticides. Compared to CPY, CPYM resulted in greater hypochromicity.

The binding strength of the pesticides to DNA can be quantitatively illustrated using fluorescence quenching of DNA–EtBr following competitive binding. In general, DNA-binding agents such as the tested pesticides compete with the fluorescent probe EtBr for binding sites on DNA molecules. Thus, a reduction in fluorescence intensity can be attributed to the separation of EtBr from the DNA base pairs in competition with DNA-binding agents (Rahban et al., 2010). This impact can be quantified by the quenching efficiency, which measures the strength of DNA binding by pesticides, and can be evaluated based on the Stern–Volmer constant (K_{SV}). Preliminary experiments had proved that no fluorescence was observed for pesticides in solution at room temperature. As shown in Fig. 3, the fluorescence intensity ratio F_0/F is linearly positively correlated with CPY or CPYM concentration, whereby the fluorescence of DNA–EtBr gradually decreased with increasing pesticide concentration. EtBr was continuously displaced from DNA base pairs by competing CPY and CPYM molecules. The higher K_{SV} value (8.02×10^6 L/mol) for CPYM, compared to that of CPY (7.73×10^6 L/mol), indicating that CPYM had a higher substitution with DNA.

Previous research using CD spectra has shown that the positive band at 275 nm due to base stacking and the negative band at 246 nm due to right-handed helicity are a typical B-DNA conformation, and sensitive to the mode of DNA interactions with binding agents (Kypr et al., 2009; Marty et al., 2009). The CD spectra (Fig. 2b) displayed two distinct bands, with the negative band at 246 nm strengthened to become more negative, and the positive band at 275 nm first increased and then decreased when DNA was incubated with CPY or CPYM at increasing concentrations. Furthermore, the similar shape of all CD spectra for treatments at different pesticide concentrations (Fig. 2b) suggested that the B-form DNA conformation did not change in the presence of pesticides.

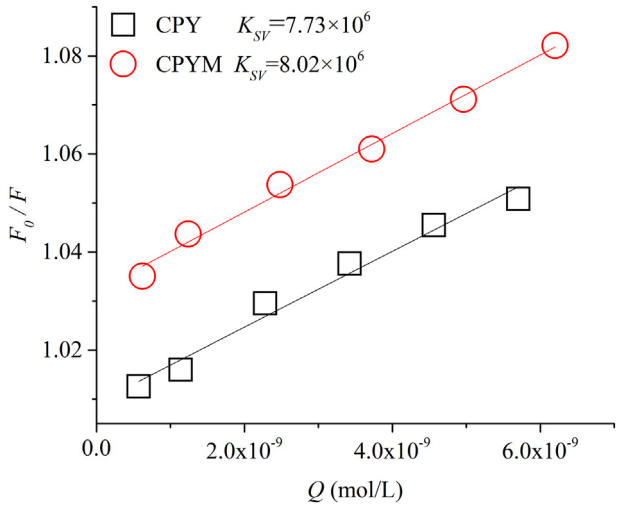

Fig. 3. Stern–Volmer plots for fluorescence quenching of ethidium bromide (EtBr) –labeled DNA by chlorpyrifos (CPY) and chlorpyrifos-methyl (CPYM). The changes in fluorescence intensity of EtBr in DNA was recorded during the CPY and CPYM titration.

The CPY and CPYM binding sites on DNA were identified through FTIR spectral changes (intensity and shifts within the 600–2000 cm^{-1} range) of DNA before and after reaction with each pesticide (Fig. 2c). Intermolecular interactions (e.g., hydrogen bonding and conjugative effects) will impact on peak position and strength (Kang et al., 2010; Shemetov et al., 2012). The vibrational bands of DNA at 1632, 1552, 1462, and 1295 cm^{-1} are assigned to the nitrogenous bases such as thymine (T), guanine (G), adenine (A), and cytosine (C), respectively. The 1213 cm^{-1} band is allocated to antisymmetric phosphoric acid stretching of the phosphate acid backbone. The intensely sharp peak at 1036 cm^{-1} is the typical absorption feature of DNA D-2-deoxyribose. The absorption band at 965 cm^{-1} indicates a B-form conformation of DNA (Banyay et al., 2003). Details of the observed absorption bands of DNA and their corresponding functional groups are provided in Table S2. Overall, no significant peak shift was observed for the vibrational bands noted above.

Fig. 2c presents the R_i values of DNA functional groups in different vibration bands in the absence and presence of CPY and CPYM. To eliminate error in the vibrational peak intensity caused by differences in the mass of the analyte in FTIR experiments, the R_i value can be corrected based on an internal reference and used to measure the degree of peak intensity change. The CD spectra shown in Fig. 2b indicated that the B-form DNA conformation was involved in binding of the two pesticides. Therefore, the intensity of the peak at 965 cm^{-1} was used as an internal reference. Compared with the R_i value of DNA + CPY and DNA + CPYM with DNA, the absorption bands of the former combination near D-2-deoxyribose (1036 cm^{-1}), C (1295 cm^{-1}), G (1552 cm^{-1}), and T (1632 cm^{-1}) were weakened. The R_i values for the C, G, and T vibrational bands in the DNA + CPYM compound changed from 0.49 to 0.43, 0.56 to 0.46, and 0.67 to 0.58, respectively. However, the DNA + CPY compound showed smaller peak intensity changes for the C and T vibrational bands and no change in the G band. Moreover, the R_i values of the D-2-deoxyribose vibrational band were reduced markedly from 2.86 to 2.66 and 2.61 in the DNA + CPY and DNA + CPYM compound, respectively. In contrast, the R_i values for the vibrational band corresponding to the DNA phosphate acid backbone were not altered by DNA binding with CPY or CPYM. This result indicated that the C and T bases and D-2-deoxyribose were the most likely DNA binding sites for CPY, while the C, G, and T bases and D-2-deoxyribose were likely binding sites for CPYM.

3.4. Simulated binding of CPY and CPYM with DNA

The DNA–CPY/CPYM interaction mechanisms observed in the laboratory experiments were subsequently simulated and confirmed using computational chemistry. Based on the spectroscopic experiments, the intercalative-binding structure containing the manually inserted pesticide molecules into the DNA base pairs (AT, GC), and docking results (groove-binding structure) as the initial structure for molecular dynamics simulation (Fig. 5a). Using the last frame of the dynamic simulation, the gradient isosurfaces and related plots of the interactive force types between the two pesticides and DNA were analyzed using the independent gradient model, and are displayed in Fig. 4a, b. These results could be used to characterize the various weak attractions between DNA and the pesticides based on isosurfaces colored on a blue–green–red scale according to values of sign(λ_2)ρ ranging from −0.05 to +0.05 au, where δg^{inter} is proportional to the binding strength of DNA and pesticides (Lefebvre et al., 2017). The blue, green, and red colors bar directly indicate attractive interactions (e.g., hydrogen bonding and halogen bonding), van der Waals interactions (e.g., dispersion force and weak repulsive force), and strong repulsive non-bonding overlap, respectively (Johnson et al., 2010).

In groove-binding mode (Fig. 4a), CPY and CPYM molecules reacted with DNA mainly through dispersion interaction, as indicated by the green isosurface area, as well as through the formation of weak

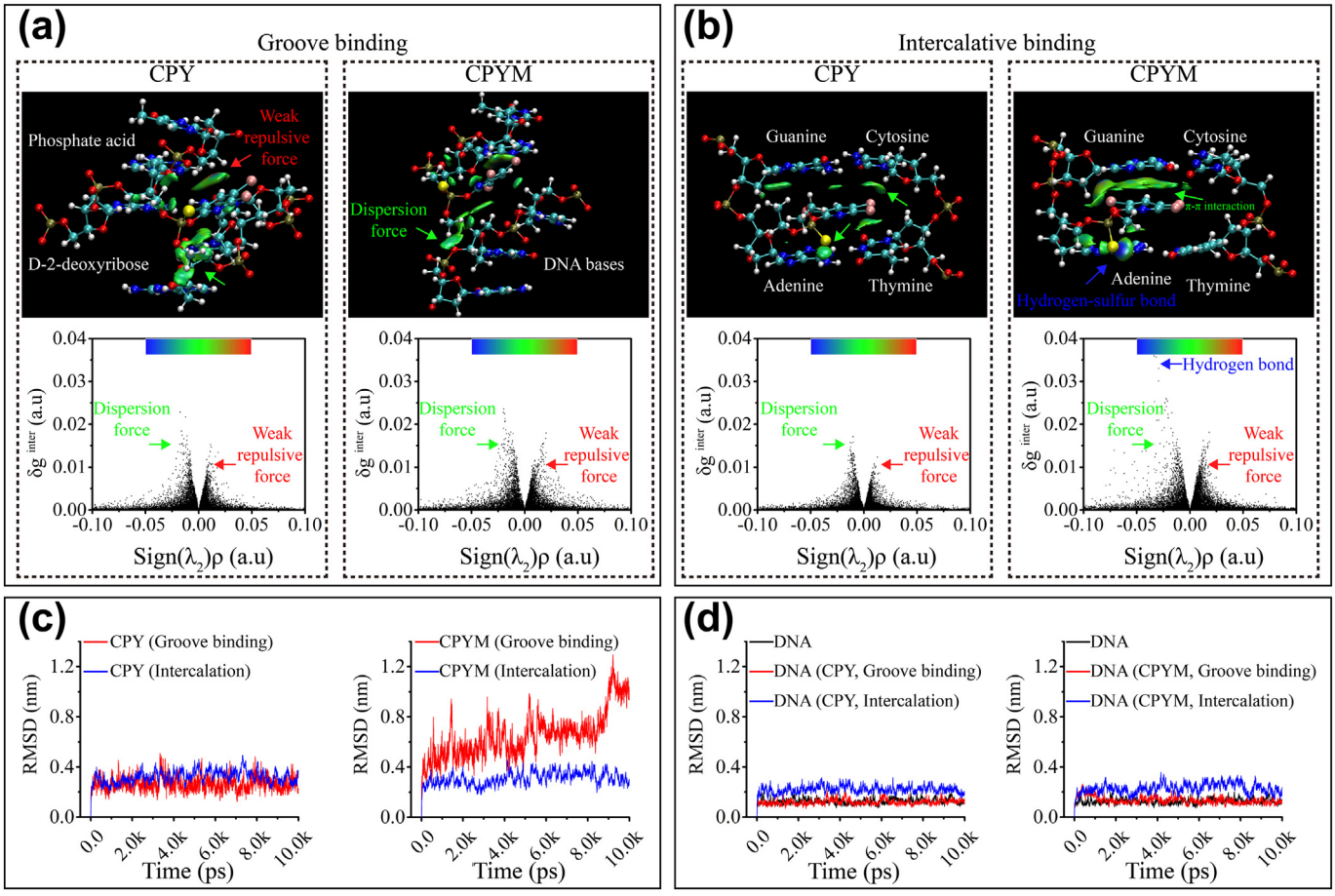

Fig. 4. Computational analysis of DNA–chlorpyrifos (CPY) and DNA–chlorpyrifos-methyl (CPYM) interactions via grooving binding and intercalation. a, b, Models illustrating the gradient isosurface of the main sections for CPY (a) and CPYM (b) interactions with DNA bases and plots of the reduced density gradient (δg^{inter}) vs. the product of electron density (ρ) and the sign of the second Hessian eigenvalue (λ_2), with surfaces colored on a blue–green–red scale according to the values and sign of (λ_2)ρ from −0.05 to +0.05 au. The blue, green, and red colors indicate attractive interactions, very weak interactions, and strong repulsive non–bonded overlap, respectively. N, H, C, O, P, S, and Cl atoms are represented in blue, white, cyan, red, copper, yellow, and pink, respectively. (c), RMSD vs. time based on molecular dynamics simulation of the binding stability between DNA and pesticides. (d), RMSD vs. time based on molecular dynamics simulation of conformational changes to DNA. (For interpretation of the references to colour in this figure legend, the reader is referred to the web version of this article.)

hydrogen–oxygen bonds with D-2-deoxyribose in DNA. In intercalative-binding mode (Fig. 4b), both CPY and CPYM showed dispersion interactions (weakening hydrogen–chlorine and hydrogen–sulfur bonds) with D-2-deoxyribose. Visual gradient isosurfaces of base–pesticide interactions showed moderate van der Waals attractions, whereby weak hydrogen–oxygen, hydrogen–chlorine, and hydrogen–sulfur dispersion interactions allowed CPY binds to C and T, while CPYM could bind to C and G. Notably, the pyridine ring of CPYM could form a significant π–π interaction with the G base of DNA, similar to the stacking of consecutive base pairs in duplex DNA, while the pyridine ring of CPY was prevented from fully entering the base pair. Overall, the computational simulations reveal that CPY and CPYM bind efficiently with bases (C, G, and T) and D-2-deoxyribose in DNA through dispersion interactions.

To evaluate the binding stability of DNA with CPY or CPYM, the root-mean-square deviation (RMSD) values of pesticides relative to DNA were calculated (Fig. 4c). Smaller RMSD values indicate more stable binding (Moraca et al., 2017; Treesuwan et al., 2009). As shown in the two plots of Fig. 4c, CPY had a stable relationship between minor grooves (RMSD = 0.27 nm) and base pairs (RMSD = 0.32 nm), while CPYM was more flexible within minor grooves (RMSD = 0.65 nm) and more stable in base pairs (RMSD = 0.31 nm). These results indicate that CPY can form a stable bond with DNA through both groove binding and intercalation, while CPYM can form a stable bond with DNA through intercalation, but bonds less stably with DNA through groove binding.

To illustrate the effects of pesticides on DNA structure, we focused on three main parameters: DNA structural disorder, DNA minor groove width, and the density of water molecules around DNA. Using pure DNA as a reference, stability in the DNA structure was evaluated using the RMSD relative to itself (Galindo-Murillo et al., 2015). The two plots in Fig. 4d show the RMSD values of DNA in the presence or absence of the pesticides. Compared with the DNA-only solution (average RMSD = 0.13 nm), intercalative binding of pesticides significantly enhanced the looseness of the DNA structure, resulting in average RMSD values of 0.22 and 0.23 nm for DNA–CPY and DNA–CPYM, respectively. In contrast, the corresponding average RMSD values for groove binding of DNA–CPY (0.12 nm) and DNA–CPYM (0.13 nm) suggest that this reaction mechanism is less effective. These results indicate that the DNA helical structure is loosened by the combination with these pesticides, primarily through intercalative binding.

The real-time distances of the major groove and minor groove of DNA are shown in Fig. 5b. The average groove distances for DNA positions throughout the whole simulation were calculated (Table S3). In groove-binding mode, fluctuations of the minor groove distance (blue line) around the binding sites (marked with black dotted rectangles) were relatively stable compared to those of DNA without the two pesticides, while major groove distances (red line) were unaffected. Furthermore, the average distances of the minor and major grooves were similar. In the intercalative-binding mode, the average distance between the minor and major grooves of DNA around the binding site increased significantly with pesticide binding. During binding with CPY

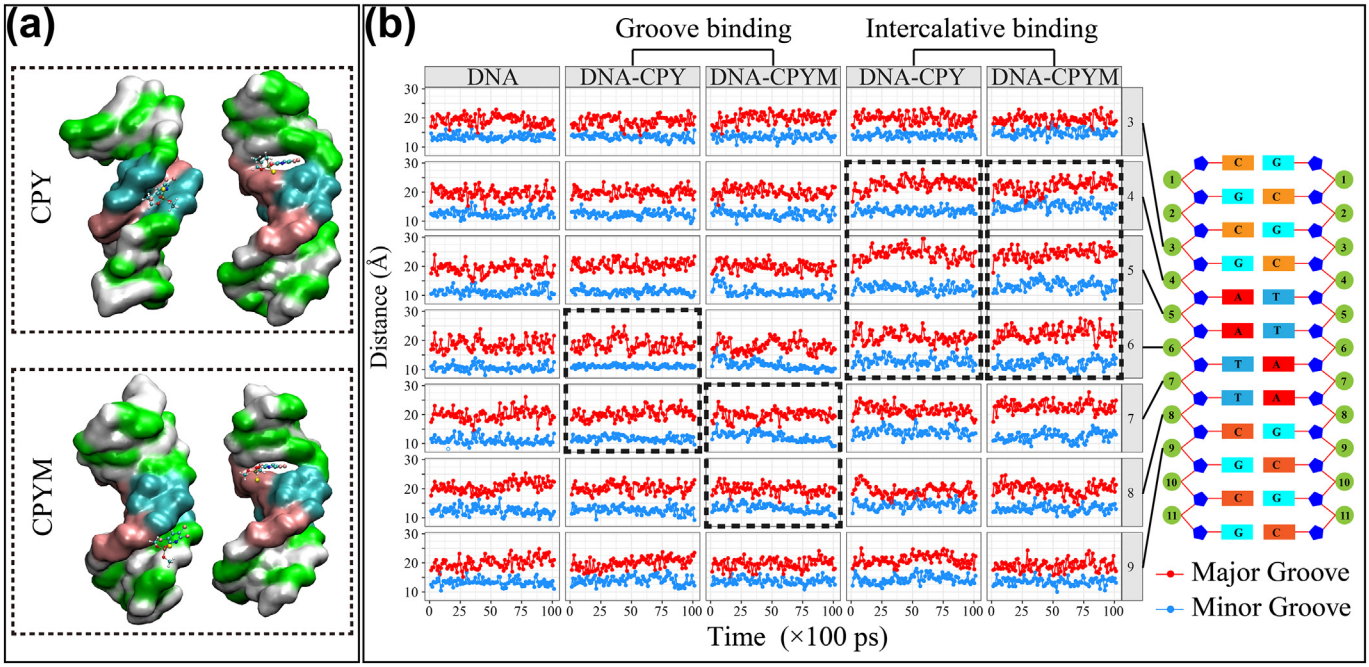

Fig. 5. Molecular dynamics simulation of real-time changes in DNA groove distance and final structures. a, Final structures from the molecular dynamics simulation of DNA–chlorpyrifos (CPY) and DNA–chlorpyrifos-methyl (CPYM) based on the groove–binding and intercalative–binding modes. b, Distance of the major and minor grooves at positions 3–9 in the DNA structure during the simulation time (10 ns). Black dotted frames indicate the distances of the DNA minor and major grooves around the binding site of the pesticide.

and CPYM, the DNA minor groove distance increased from 12.69 to 13.53 and 15.12 Å (position number 4), 11.22 to 12.44 and 13.35 Å (position number 5), and 10.61 to 12.87 and 12.14 Å (position number 6), respectively, while the major groove distance at the corresponding position was also extended by 3.00 and 2.36 Å (position number 4), 5.01 and 5.06 Å (position number 5), and 2.65 and 3.76 Å (position number 6) (Table S3). This result suggests that groove binding between DNA and the two pesticides generally stabilizes the minor groove width, while intercalation enlarges the minor and major groove distances, supporting the loosening of the DNA structure.

The radial distribution function was used to calculate the probability g(r) of water molecules being present at a certain distance (r) from a DNA molecule (Fig. 6):

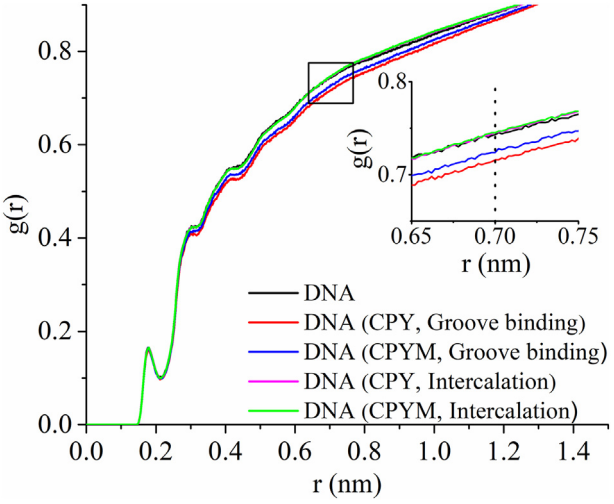

Fig. 6. Water molecular presence probability g(r) vs. DNA distance (r) from the radial distribution function of the water density distribution surrounding DNA molecules. The insert is an enlargement of the section outlined with the black box around the DNA distance of 0.7 nm.

$$g(r) = \frac{n(r)}{4\pi r^2 dr\left(\frac{N}{V}\right)} \quad (2)$$

where N is the total number of water molecules, V is the system volume, and n(r) is the number of water molecules within the range r ± Δr/2. DNA double helix has an average radius of 1.0 nm, the probabilities of water molecules between 0– and 1.0 nm can be used to characterize the presence of water molecules in DNA grooves. We used the probability of water molecules 0.7 nm from the center of mass of a DNA molecule as an example (Fig. 6). For groove binding of DNA with CPY and CPYM, the probabilities of water molecules appearing around the DNA molecule were 0.716 and 0.724, respectively, both lower than that for DNA in the absence of pesticides (0.743). Meanwhile, there was a non-significant change in the probability (0.745) of water molecules existing around a DNA molecule bound to CPY or CPYM through intercalation. Because both CPY and CPYM are hydrophobic, their interaction with DNA through groove binding may significantly reduce the probability of water molecules surrounding the DNA molecule, resulting in dehydration of the DNA grooves.

4. Discussion

The quantification of the relationships between eDNA degradation and the environmental contaminant has not yet been determined; however, degradation is likely associated with DNA deformation and hydrophobicity (Brukner et al., 1990; McDermott et al., 2017). In this study, our goal was to use spectroscopic and computational chemistry techniques that explored DNA deformation and hydrophobicity while further elucidating the mechanism of CPY- and CPYM- promoted enzymatic degradation of DNA. Research carried out on DNA degradation rates has been scanty; however, this is one of the first studies (see Kang et al., 2010) to consider the degradation of DNA by organic contaminants, and we expect this approach to be valuable for affecting species diversity and ecotoxicology in aqueous systems.

4.1. Physicochemical characteristics of DNA in the presence of pesticides

The insertion of the CPY and CPYM molecules into DNA base pairs likely results in the destruction of these conjugated structures and the overlapping π electron cloud of the DNA bases, resulting in the observed hypochromicity (Karami et al., 2018; Kesavan et al., 2017; Nwokeoji et al., 2017; Shujha et al., 2010). Pyridine ring-containing compounds (e.g., 2-amino-1-methyl-6-phenylimidazo[4,5-*b*]pyridine and 2,2-dipyridyl) have been reported to intercalate into DNA base pairs (Andersson et al., 2013; Brown et al., 2001), suggesting that the binding pocket of DNA could permit CPY and CPYM, which also contain pyridine ring structure, to be substituted EtBr molecule between base pairs of the tested double-stranded DNA.

The orientation of the induced peak is often correlated with the binding mode of DNA-binding agents. Groove binders have been reported to cause a powerful positive change in the CD spectrum, whereas intercalating agents can lead to a negative shift in the CD spectrum (Grueso et al., 2012; Hebenbrock et al., 2018). The negative strengthening of the 246 nm band reveals an intercalative binding mode between DNA and the two pesticides, as well as the buckling of the right-handed helicity with increasing pesticides concentration. Increased base stacking due to intercalation of planar molecules into DNA base pairs has been confirmed previously (Qais et al., 2017). Because both positive and negative peak vibrations were observed in the CD spectra, it is highly likely that CPY and CPYM interact with DNA in both groove-binding and intercalative binding coexistent mode (at low pesticide concentrations) and an intercalative binding mode (at high pesticide concentrations).

Multiple atoms (chlorine, sulfur, nitrogen and oxygen atoms) in CPY and CPYM molecules could act as weak hydrogen bond donors or acceptors. Besides, the weak hydrogen bond formation would cause the electric polarity migration of base-pesticide conjugated structures to weaken the dipole moment of DNA functional groups. It was reported that binding of various functional groups in DNA by carboplatin and oxovanadium ions could decrease the dipole moment between the bonding atoms at the binding site, resulting in decreased absorbance intensity in the vibrational bands of the affected DNA functional groups (Ahmed Ouameur et al., 2006; Jangir et al., 2010). The FTIR data proved that two pesticides bind with DNA through the weak hydrogen bond, weakening the dipole moment of functional groups.

4.2. Mechanism of CPY- and CPYM-promoted enzymatic degradation of DNA

Using molecular dynamics simulation, we obtained information on the DNA deformation and pesticides binding sites at the molecular level. The indirect exploration of DNA structure by pesticide molecules can also explain its mechanism of promoting DNA enzymatic degradation. In the analysis of the interaction force between the pesticide and the DNA binding site, the binding site is surprisingly consistent with the results of the FTIR spectrum; pesticides are bound with C, G, T bases and D-2-deoxyribose via dispersion interactions. CPYM is unstable in DNA grooves when assessing binding stability. However, the conformation advantage makes CPYM easier to intercalate the base pairs and stabilize by π–π interaction, making up for the lack of instability in the groove binding. Interestingly, the doubling of the rise, buckling of the base pairs flanking the intercalation site in intercalative-binding mode, which verified the changes of DNA base stacking and right-handed helicity in CD spectrum. Deformation and hydrophobicity are the main factors that may cause differences in DNA degradation. Ivan Brukner et al. found that the expansion of the DNA minor groove led to easier recognition by DNase I (Brukner et al., 1990). Moreover, the findings of McDermott et al. showed that non-polar molecules could destroy the hydration layer structure around DNA (McDermott et al., 2017). Additionally, Jayaram et al. proposed that water released from DNA interfaces would favor protein–DNA binding (Jayaram and Jain, 2004). Altogether, the simulation results have confirmed that, in the presence of pesticide molecules, the groove width of DNA is enlarged, and the hydration layer on the DNA surface is destroyed, which is the main factor of DNase I to recognition DNA.

5. Conclusions

Collectively, this set of experiments advances understanding of some factors and processes that promote eDNA degradation when organophosphorus pesticides were released into the environment and coexisted with eDNA. The enhanced hydrophobicity of the DNA groove upon binding with CPY and CPYM promotes the recognition and binding of DNA by DNase I. Meanwhile, both CPY and CPYM can expand the distance of the DNA groove through intercalation. The expansion further contributes to binding of the DNase I functional domain to the minor groove and facilitating the DNA strand-cutting action of DNase I, thus, ultimately enhancing eDNA degradation in the presence of CPY or CPYM. Our results suggest that legacy pesticides such as organophosphorus pesticides may regulate residual genes in our environment. This investigation uncovers the beneficial approach of combining experimental observations with molecular computation on interactions of eDNA and contaminants in the understanding of the interface mechanism and risks of both DNA and contaminants. In future studies, the relationship between eDNA and target pollutant in natural aquatic environments needs to be further studied. Also, eDNA is more heterogeneous and could also be bound to other molecules (e.g., protein, polysaccharide), which can alter the accessibility of CPY/CPYM to the DNA. It is, therefore, necessary to place the in vitro results in the context of more complicated aqueous systems.

Declaration of competing interest

The authors declare no competing interests with the contents of this article.

Acknowledgments

This work was supported by the National Natural Science Foundation of China (41877125, 41771523), and the Jiangsu Provincial Key Research and Development Program, China (BE2017718). We are grateful for computation resources from the High-Performance Computing System at National Engineering Laboratory of Soil Pollution Control and Remediation Technologies, CAS Key Laboratory of Soil Environment and Pollution Remediation, Institute of Soil Science, Chinese Academy of Sciences.

Appendix A. Supplementary data

Supplementary data to this article can be found online at https://doi.org/10.1016/j.envint.2019.105087.

References

Ahmed Ouameur, A., Arakawa, H., Tajmir-Riahi, H.A., 2006. Binding of oxovanadium ions to the major and minor grooves of DNA duplex: stability and structural models. Biochem. Cell Biol. 84, 677–683.

Andersson, J., Fornander, L.H., Abrahamsson, M., Tuite, E., Nordell, P., Lincoln, P., 2013. Lifetime heterogeneity of DNA-bound dppz complexes originates from distinct intercalation geometries determined by complex-complex interactions. Inorg. Chem. 52, 1151–1159.

Banyay, M., Sarkar, M., Gräslund, A., 2003. A library of IR bands of nucleic acids in solution. Biophys. Chem. 104, 477–488.

Barnes, M.A., Turner, C.R., Jerde, C.L., Renshaw, M.A., Chadderton, W.L., Lodge, D.M., 2014. Environmental conditions influence eDNA persistence in aquatic systems. Environ. Sci. Technol. 48, 1819–1827.

Borin, S., Crotti, E., Mapelli, F., Tamagnini, I., Corselli, C., Daffonchio, D., 2008. DNA is preserved and maintains transforming potential after contact with brines of the deep anoxic hypersaline lakes of the Eastern Mediterranean Sea. Aquat. Biosyst. 4, 10.

Brown, K., Hingerty, B.E., Guenther, E.A., Krishnan, V.V., Broyde, S., Turteltaub, K.W.,

Cosman, M., 2001. Solution structure of the 2-amino-1-methyl-6-phenylimidazo[4,5-b]pyridine C8-deoxyguanosine adduct in duplex DNA. Proc. Natl. Acad. Sci. U. S. A. 98, 8507–8512.
Brukner, I., Jurukovski, V., Savic, A., 1990. Sequence-dependent structural variations of DNA revealed by DNase I. Nucleic Acids Res. 18, 891–894.
Bylemans, J., Furlan, E.M., Gleeson, D.M., Hardy, C.M., Duncan, R.P., 2018. Does size matter? An experimental evaluation of the relative abundance and decay rates of aquatic environmental DNA. Environ. Sci. Technol. 52, 6408–6416.
Corinaldesi, C., Danovaro, R., Dell'Anno, A., 2005. Simultaneous recovery of extracellular and intracellular DNA suitable for molecular studies from marine sediments. Appl. Environ. Microbiol. 71, 46–50.
Demanèche, S., Jocteur-Monrozier, L., Quiquampoix, H., Simonet, P., 2001. Evaluation of biological and physical protection against nuclease degradation of clay-bound plasmid DNA. Proc. Natl. Acad. Sci. U. S. A. 67, 293–299.
Dick, L.K., Stelzer, E.A., Bertke, E.E., Fong, D.L., Stoeckel, D.M., 2010. Relative decay of *Bacteroidales* microbial source tracking markers and cultivated *Escherichia coli* in freshwater microcosms. Appl. Environ. Microbiol. 76, 3255–3262.
Flemming, H.C., Wingender, J., Szewzyk, U., Steinberg, P., Rice, S.A., Kjelleberg, S., 2016. Biofilms: an emergent form of bacterial life. Nat. Rev. Microbiol. 14, 563–575.
Galindo-Murillo, R., Roe, D.R., Cheatham III, T.E., 2015. Convergence and reproducibility in molecular dynamics simulations of the DNA duplex d (GCACGAACGAACGAACGC). Biochim. Biophys. Acta, Gen. Subj. 1850, 1041–1058.
Giesy, J.P., Solomon, K.R., 2014. Ecological Risk Assessment for Chlorpyrifos in Terrestrial and Aquatic Systems in the United States. Springer International Publishing, United States.
Grueso, E., Cerrillos, C., Hidalgo, J., Lopez-Cornejo, P., 2012. Compaction and decompaction of DNA induced by the cationic surfactant CTAB. Langmuir 28, 10968–10979.
Hebenbrock, M., González-Abradelo, D., Strassert, C.A., Müller, J., 2018. DNA groove-binding ability of luminescent platinum(II) complexes based on a family of tridentate N^N^C ligands bearing differently substituted alkyl tethers. Z. Anorg. Allg. Chem. 644, 671–682.
Hua, X., Qian, G., Yang, J., Hu, B., Fan, J., Qin, N., Li, G., Wang, Y., Liu, F., 2010. Development of an immunochromatographic assay for the rapid detection of chlorpyrifos-methyl in water samples. Biosens. Bioelectron. 26, 189–194.
Humphrey, W., Dalke, A., Schulten, K., 1996. VMD: visual molecular dynamics. J. Mol. Graph. 14, 33–38.
Ibáñez de Aldecoa, A.L., Zafra, O., González-Pastor, J.E., 2017. Mechanisms and regulation of extracellular DNA release and its biological roles in microbial communities. Front. Microbiol. 8, 1390.
Jangir, D.K., Tyagi, G., Mehrotra, R., Kundu, S., 2010. Carboplatin interaction with calf-thymus DNA: a FTIR spectroscopic approach. J. Mol. Struct. 969, 126–129.
Jayaram, B., Jain, T., 2004. The role of water in protein-DNA recognition. Annu. Rev. Biophys. Biomol. Struct. 33, 343–361.
Johnson, E.R., Keinan, S., Mori-Sanchez, P., Contreras-Garcia, J., Cohen, A.J., Yang, W., 2010. Revealing noncovalent interactions. J. Am. Chem. Soc. 132, 6498–6506.
Kang, F., Gao, Y., Wang, Q., 2010. Inhibition of free DNA degradation by the deformation of DNA exposed to trace polycyclic aromatic hydrocarbon contaminants. Environ. Sci. Technol. 44, 8891–8896.
Kang, F., Hu, X., Liu, J., Gao, Y., 2015. Noncovalent binding of polycyclic aromatic hydrocarbons with genetic bases reducing the *in vitro* lateral transfer of antibiotic resistant genes. Environ. Sci. Technol. 49, 10340–10348.
Karami, K., Alinaghi, M., Amirghofran, Z., Lipkowski, J., Momtazi-borojeni, A.A., 2018. A saccharinate-bridged palladacyclic dimer with a Pd–Pd bond: experimental and molecular docking studies of the interaction with DNA and BSA and *in vitro* cytotoxicity against human cancer cell lines. New J. Chem. 42, 574–586.
Kashanian, S., Shariati, Z., Roshanfekr, H., Ghobadi, S., 2012. DNA binding studies of 3, 5, 6-trichloro-2-pyridinol pesticide metabolite. DNA Cell Biol. 31, 1341–1348.
Kesavan, M.P., Vinoth Kumar, G.G., Dhaveethu Raja, J., Anitha, K., Karthikeyan, S., Rajesh, J., 2017. DNA interaction, antimicrobial, antioxidant and anticancer studies on Cu(II) complexes of Luotonin A. J. Photochem. Photobiol. B 167, 20–28.
Koureas, M., Tsakalof, A., Tsatsakis, A., Hadjichristodoulou, C., 2012. Systematic review of biomonitoring studies to determine the association between exposure to organophosphorus and pyrethroid insecticides and human health outcomes. Toxicol. Lett. 210, 155.
Kovačić, I., Medić, N., 2016. The effect of chlorpyrifos on protein content and acid DNase activity in the mussel, *Mytilus galloprovincialis*. Mar. Freshwater Behav. Physiol. 49, 265–275.
Kumar, R., Grubmüller, H., 2015. do_x3dna: a tool to analyze structural fluctuations of dsDNA or dsRNA from molecular dynamics simulations. Bioinformatics 31, 2583–2585.
Kypr, J., Kejnovska, I., Renciuk, D., Vorlickova, M., 2009. Circular dichroism and conformational polymorphism of DNA. Nucleic Acids Res. 37, 1713–1725.
Lefebvre, C., Rubez, G., Khartabil, H., Boisson, J.C., Contreras-García, J., Hénon, E., 2017. Accurately extracting the signature of intermolecular interactions present in the NCI plot of the reduced density gradient versus electron density. Phys. Chem. Chem. Phys. 19, 17928–17936.
Lu, T., Chen, F., 2012. Multiwfn: a multifunctional wavefunction analyzer. J. Comput. Chem. 33, 580–592.
Ma, F., Ma, Y., Du, C., Yang, X., Shen, R., 2015. Comparison on the interaction of Al^{3+}/nano-Al_{13} with calf thymus DNA/salmon sperm DNA. J. Mol. Struct. 1100, 154–161.
Mao, D., Luo, Y., Mathieu, J., Wang, Q., Feng, L., Mu, Q., Feng, C., Alvarez, P.J., 2014. Persistence of extracellular DNA in river sediment facilitates antibiotic resistance gene propagation. Environ. Sci. Technol. 48, 71–78.
Marty, R., N'Soukpoe-Kossi, C.N., Charbonneau, D., Weinert, C.M., Kreplak, L., Tajmir-Riahi, H.A., 2009. Structural analysis of DNA complexation with cationic lipids. Nucleic Acids Res. 37, 849–857.
Matsui, K., Honjo, M., Kawabata, Z.i., 2001. Estimation of the fate of dissolved DNA in thermally stratified lake water from the stability of exogenous plasmid DNA. Aquat. Microb. Ecol. 26, 95–102.
McDermott, M.L., Vanselous, H., Corcelli, S.A., Petersen, P.B., 2017. DNA's chiral spine of hydration. ACS Cent. Sci. 3, 708–714.
Moraca, F., Amato, J., Ortuso, F., Artese, A., Pagano, B., Novellino, E., Alcaro, S., Parrinello, M., Limongelli, V., 2017. Ligand binding to telomeric G-quadruplex DNA investigated by funnel-metadynamics simulations. Proc. Natl. Acad. Sci. U. S. A. 114, 2136–2145.
Morris, G.M., Goodsell, D.S., Halliday, R.S., Huey, R., Hart, W.E., Belew, R.K., Olson, A.J., 1998. Automated docking using a Lamarckian genetic algorithm and an empirical binding free energy function. J. Comput. Chem. 19, 1639–1662.
Morris, G.M., Huey, R., Lindstrom, W., Sanner, M.F., Belew, R.K., Goodsell, D.S., Olson, A.J., 2009. AutoDock4 and AutoDockTools4: automated docking with selective receptor flexibility. J. Comput. Chem. 30, 2785–2791.
Nielsen, K.M., Johnsen, P.J., Bensasson, D., Daffonchio, D., 2007. Release and persistence of extracellular DNA in the environment. Environ. Biosaf. Res. 6, 37–53.
Nwokeoji, A.O., Kilby, P.M., Portwood, D.E., Dickman, M.J., 2017. Accurate quantification of nucleic acids using hypochromicity measurements in conjunction with UV spectrophotometry. Anal. Chem. 89, 13567–13574.
Okabe, S., Shimazu, Y., 2007. Persistence of host-specific *Bacteroides–Prevotella* 16S rRNA genetic markers in environmental waters: effects of temperature and salinity. Appl. Microbiol. Biotechnol. 76, 935–944.
Páll, S., Abraham, M.J., Kutzner, C., Hess, B., Lindahl, E., 2015. Tackling Exascale Software Challenges in Molecular Dynamics Simulations With GROMACS. Springer International Publishing, Cham.
Ponnuswamy, N., Bastings, M.M., Nathwani, B., Ryu, J.H., Chou, L.Y., Vinther, M., Li, W.A., Anastassacos, F.M., Mooney, D.J., Shih, W.M., 2017. Oligolysine-based coating protects DNA nanostructures from low-salt denaturation and nuclease degradation. Nat. Commun. 8, 15654.
Popov, A.P., Konichev, A.S., Tsvetkov, I.L., 2003. Effect of toxic industrial pollutants on the activity and isoforms of acid DNase in the freshwater snail *Viviparus viviparus* L. Appl. Biochem. Microbiol. 39, 454–458.
Qais, F.A., Abdullah, K.M., Alam, M.M., Naseem, I., Ahmad, I., 2017. Interaction of capsaicin with calf thymus DNA: a multi-spectroscopic and molecular modelling study. Int. J. Biol. Macromol. 97, 392–402.
Qin, C., Yang, B., Zhang, W., Ling, W., Liu, C., Liu, J., Li, X., Gao, Y., 2019. Organochlorinated pesticides expedite the enzymatic degradation of DNA. Commun. Biol. 2, 81.
Rahban, M., Divsalar, A., Saboury, A.A., Golestani, A., 2010. Nanotoxicity and spectroscopy studies of silver nanoparticle: calf thymus DNA and K562 as targets. J. Phys. Chem. C 114, 5798–5803.
Saeki, K., Ihyo, Y., Sakai, M., Kunito, T., 2011. Strong adsorption of DNA molecules on humic acids. Environ. Chem. Lett. 9, 505–509.
Sambrook, J., Fritsch, E.F., Maniatis, T., 1989. Molecular Cloning: A Laboratory Manual. Cold spring harbor laboratory press.
Shemetov, A.A., Nabiev, I., Sukhanova, A., 2012. Molecular interaction of proteins and peptides with nanoparticles. ACS Nano 6, 4585–4602.
Shujha, S., Shah, A., Zia Ur, R., Muhammad, N., Ali, S., Qureshi, R., Khalid, N., Meetsma, A., 2010. Diorganotin(IV) derivatives of ONO tridentate Schiff base: synthesis, crystal structure, *in vitro* antimicrobial, anti-leishmanial and DNA binding studies. Eur. J. Med. Chem. 45, 2902–2911.
Sun, A.L., Zhang, Y.F., Sun, G.P., Wang, X.N., Tang, D., 2017. Homogeneous electrochemical detection of ochratoxin A in foodstuff using aptamer-graphene oxide nanosheets and DNase I-based target recycling reaction. Biosens. Bioelectron. 89, 659–665.
Tanaka, K., Okahata, Y., 1996. A DNA−lipid complex in organic media and formation of an aligned cast film[1]. J. Am. Chem. Soc. 118, 10679–10683.
Thomas, C.M., Nielsen, K.M., 2005. Mechanisms of, and barriers to, horizontal gene transfer between bacteria. Nat. Rev. Microbiol. 3, 711–721.
Tomar, P.P.S., Nikhil, K., Singh, A., Selvakumar, P., Roy, P., Sharma, A.K., 2014. Characterization of anticancer, DNase and antifungal activity of pumpkin 2S albumin. Biochem. Biophys. Res. Commun. 448, 349–354.
Torti, A., Lever, M.A., Jorgensen, B.B., 2015. Origin, dynamics, and implications of extracellular DNA pools in marine sediments. Mar. Genomics 24, 185–196.
Treesuwan, W., Wittayanarakul, K., Anthony, N.G., Huchet, G., Alniss, H., Hannongbua, S., Khalaf, A.I., Suckling, C.J., Parkinson, J.A., Mackay, S.P., 2009. A detailed binding free energy study of 2:1 ligand-DNA complex formation by experiment and simulation. Phys. Chem. Chem. Phys. 11, 10682–10693.
Trunnelle, K.J., Bennett, D.H., Tulve, N.S., Clifton, M.S., Davis, M.D., Calafat, A.M., Moran, R., Tancredi, D.J., Hertz-Picciotto, I., 2014. Urinary pyrethroid and chlorpyrifos metabolite concentrations in Northern California families and their relationship to indoor residential insecticide levels, part of the Study of Use of Products and Exposure Related Behavior (SUPERB). Environ. Sci. Technol. 48, 1931–1939.
Wang, J., Wang, W., Kollman, P.A., Case, D.A., 2006. Automatic atom type and bond type perception in molecular mechanical calculations. J. Mol. Graphics Modell. 25, 247–260.
Whitchurch, C.B., Tolker-Nielsen, T., Ragas, P.C., Mattick, J.S., 2002. Extracellular DNA required for bacterial biofilm formation. Science 295, 1487.
Williams, W.M., Giddings, J.M., Purdy, J., Solomon, K.R., Giesy, J.P., 2014. Exposures of aquatic organisms to the organophosphorus insecticide, chlorpyrifos resulting from use in the United States. Rev. Environ. Contam. Toxicol.s 231, 77–117.